LAHET™ Benchmark Calculations for Protons Incident on ^{90}Zr and ^{208}Pb

R.E. Prael
Los Alamos National Laboratory
(USA)

Abstract

A new and correct set of LAHET benchmark calculations have been prepared for submission to an international code comparison. The calculated data are presented in graphical form for comparison with previously published calculations and experimental data. The LAHET calculations were made using a multistage, multistep preequilibrium exciton model following the Bertini intranuclear cascade model and preceding the evaporation stage.

1. Introduction

This volume contains a summary, in graphs, of the results calculated using LAHET™ [1] for an international code comparison for intermediate energy nuclear data. The results originally submitted, and subsequently published[2], were incorrect; as a result of error, the previous LAHET results correspond to incident *neutrons* rather than incident protons. A complete tabulation of the proper calculated results is available from the author.

2. The Models Used

Since LAHET has several options for the physics models, it is necessary to specify those chosen for this set of calculations. The intranuclear cascade model is that of Bertini[3], the evaporation model that of Dresner[4], and the fission model (for ^{208}Pb) that of Atchison[5]. A multistage, multistep preequilibrium exciton model[6] ("MPM") acts between the cascade and the evaporation stages. The level density parameter a, for the preequilibrium and evaporation phases, is obtained from the energy dependent formulation of Ignatyuk[7] as implemented in GNASH[8].

The preequilibrium option employed is one that has previously been called the "hybrid MPM"[9,10]. A random selection is made at each collision for choosing a "pure MPM" mode with probability P, wherein the cascade products are discarded and emission is obtained from the MPM starting in a 2P-1H configuration. The probability for the pure MPM is given by $P = \min[E_1/E_c, 1.0]$, where E_c is the incident energy and $E_1 = 25$MeV. Otherwise, the MPM is invoked following the completion of the cascade phase ("normal MPM").

The effect of this particular implementation of the MPM is readily seen in the following plots. At 25 MeV incident particle energy, *all* preevaporation emission comes via the MPM. At 256 MeV incident particle energy, about 90% of interactions allow full emission by the Bertini INC model. Thus the typical INC quasielastic peak at forward angles vanishes as the incident energy is reduced to 25 MeV.

A fuller discussion of the physics models of LAHET is provided in a companion paper.[11]

3. Conclusions

A comparison of these new calculations with the published benchmark data[2] shows that the use of the correct incident particle improves agreement, as would be expected. In addition, since LAHET conserves energy with respect to real target masses for quasielastic events, the high energy edge of the (p,xn) cross sections vanishes at the proper energy. The use of the "hybrid MPM" option eliminates the INC quasielastic peak at low energies, which is desirable, but it appears in its typical over-narrow form as the incident energy increases.

However, the coupling of the MPM with the Bertini model in general leads to too much preequilibrium emission, observed at the back angles. This effect results from using a minimally low exciton state as the initial condition for the MPM following the cascade phase, and could be improved with a more sophisticated algorithm.

Another defect may be noted, in that back angle emission from the MPM is nearly uniform at angles from 120° to 180° . As presently coded, the Kalbach systematics are applied to the angular distribution of the emitted particle only for first stage emission; isotropic (C of M) emission is used otherwise. Thus, the anisotropic distribution is employed only when *no* particle is emitted in the cascade phase.

4. References

1. Richard E. Prael and Henry Lichtenstein, "User Guide to LCS: The LAHET Code System", LA-UR-89-3014, Los Alamos National Laboratory (September 1989).
2. M. Blann et. al., *International Code Comparison for Intermediate Energy Nuclear Data*, Nuclear Energy Agency, OECD, Paris (1994).
3. H. W. Bertini, *Phys. Rev. 188* (1969), p. 1711.
4. L. Dresner,"EVAP – A Fortran Program for Calculating the Evaporation of Various Particles from Excited Compound Nuclei", ORNL-TM-196, Oak Ridge National Laboratory (April 1962).
5. F. Atchison, "Spallation and Fission in Heavy Metal Nuclei under Medium Energy Proton Bombardment", in *Targets for Neutron Beam Spallation Sources*, Jül-Conf-34, Kernforschungsanlage Jülich GmbH (January 1980).
6. R. E. Prael and Michael Bozoian, "Adaptation of the Multistage Preequilibrium Model for the Monte Carlo Method (I)", LA-UR-88-3238, Los Alamos National Laboratory (September 1988).
7. A. V. Ignatyuk, G. N. Smirenkin, and A. S. Tishin, *Sov. J. Nucl. Phys. 21* (1975), p. 256.
8. E. D. Arthur,"The GNASH Preequilibrium-Statistical Model Code", LA-UR-88-382, Los Alamos National Laboratory (February 1988).
9. R. E. Prael, "LAHET Benchmark Calculations of Differential Neutron Production Cross Sections for 113 MeV and 256 MeV Protons", LA-UR-89-3347, Los Alamos National Laboratory (September 1989).
10. R. E. Prael, "LAHET Benchmark Calculations of Neutron Yields from from Stopping-Length Targets for 113 MeV and 256 MeV Protons", LA-UR-90-1620, Los Alamos National Laboratory (May 1990).
11. R. E. Prael,"A Review of Physics Models in the LAHET^{TM} Code", submitted for *Specialists' Meeting on Intermediate Energy Nuclear Data*, Nuclear Energy Agency, OECD, Paris, May 30 - June 1, 1994, LA-UR-94-1796, Los Alamos National Laboratory (May 1994).

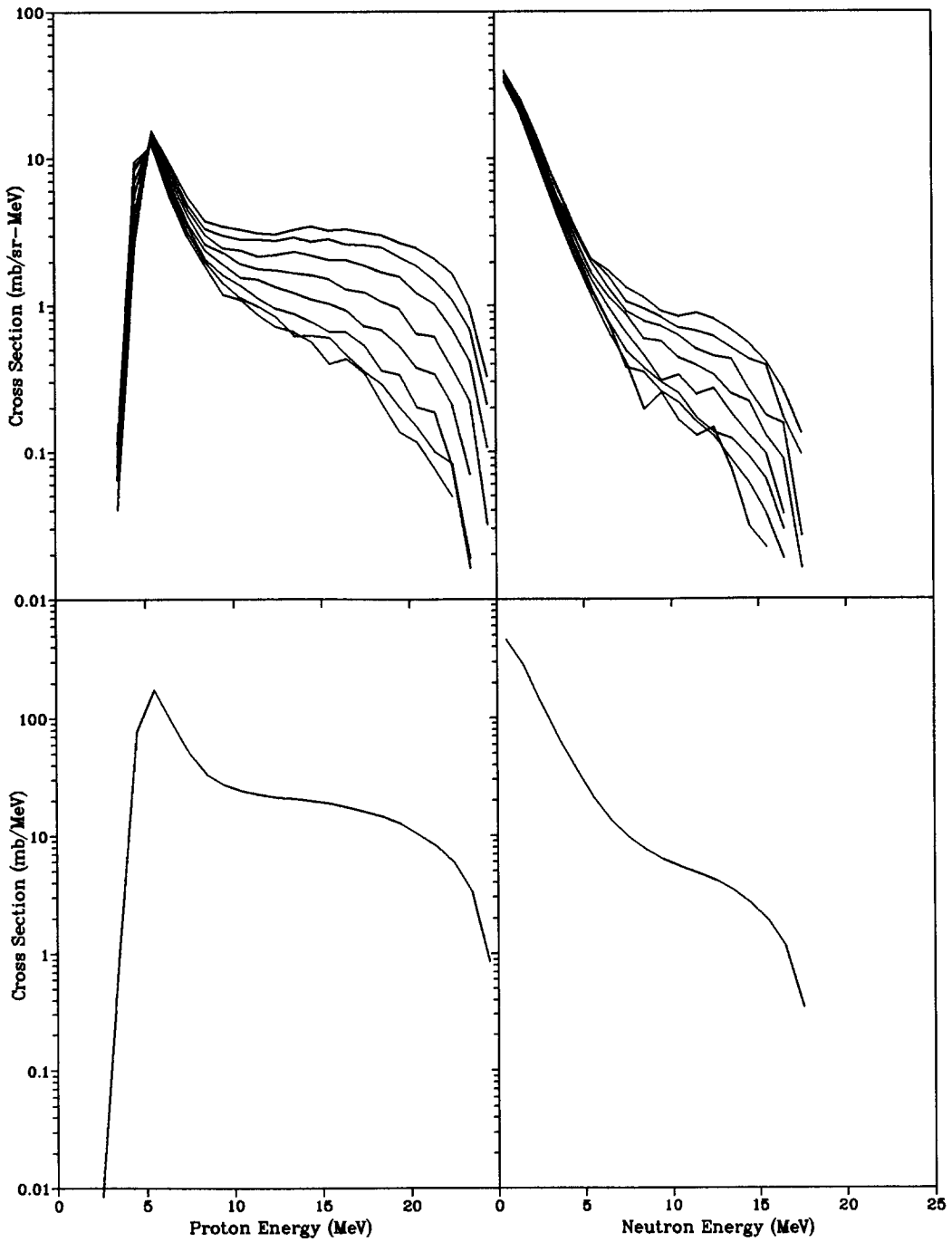

Figure 1: 25 MeV protons on ^{90}Zr. Upper left: proton emission spectrum at 20° , 40° , 60° , 80° , 100° , 120° , 140° , and 160° . Upper right: neutron emission spectrum at same angles. Lower left: angle integrated proton emission spectrum. Lower right: angle integrated neutron emission spectrum.

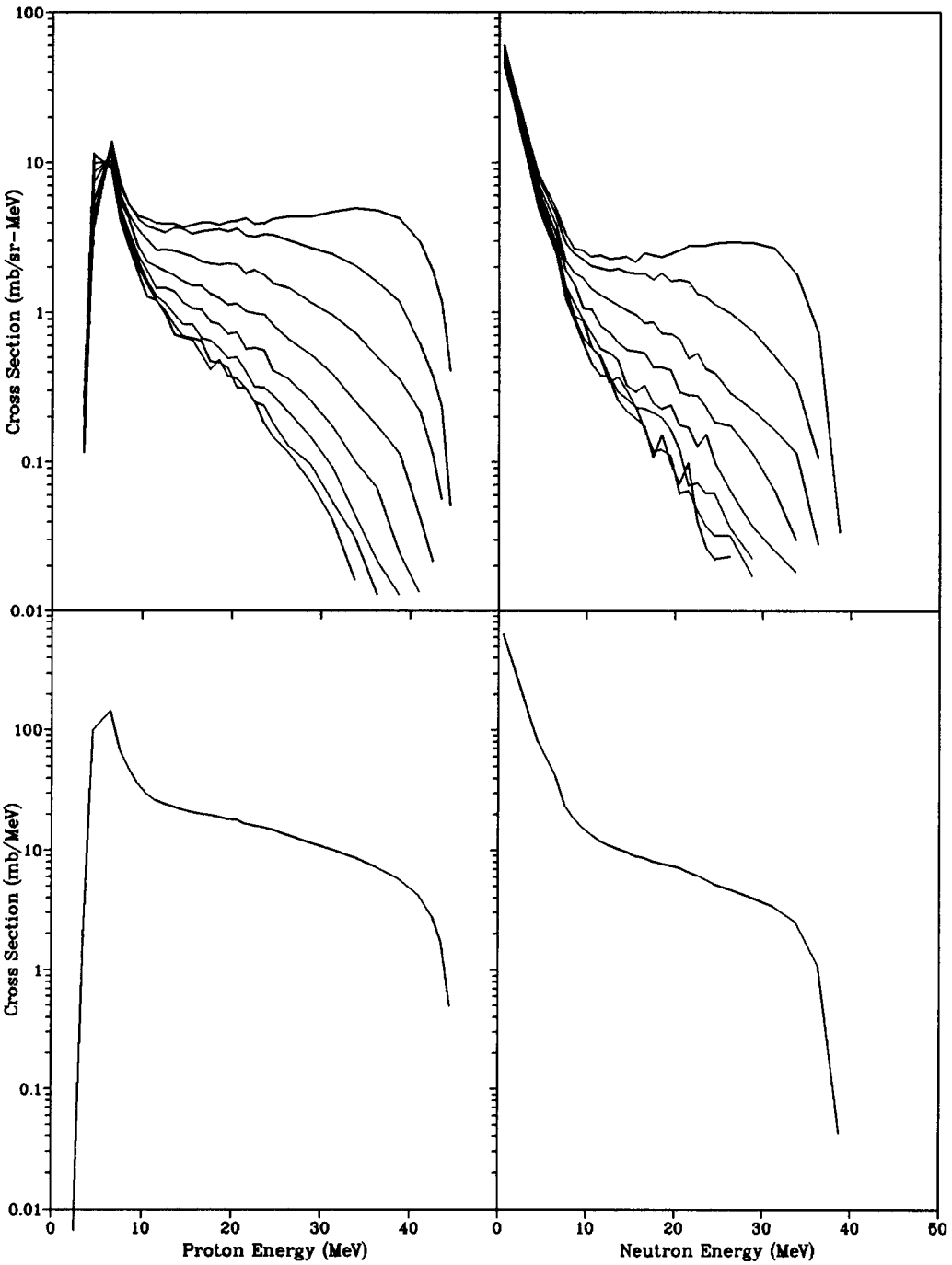

Figure 2: 45 MeV protons on ^{90}Zr. Upper left: proton emission spectrum at 20° , 40° , 60° , 80° , 100° , 120° , 140° , and 160° . Upper right: neutron emission spectrum at same angles. Lower left: angle integrated proton emission spectrum. Lower right: angle integrated neutron emission spectrum.

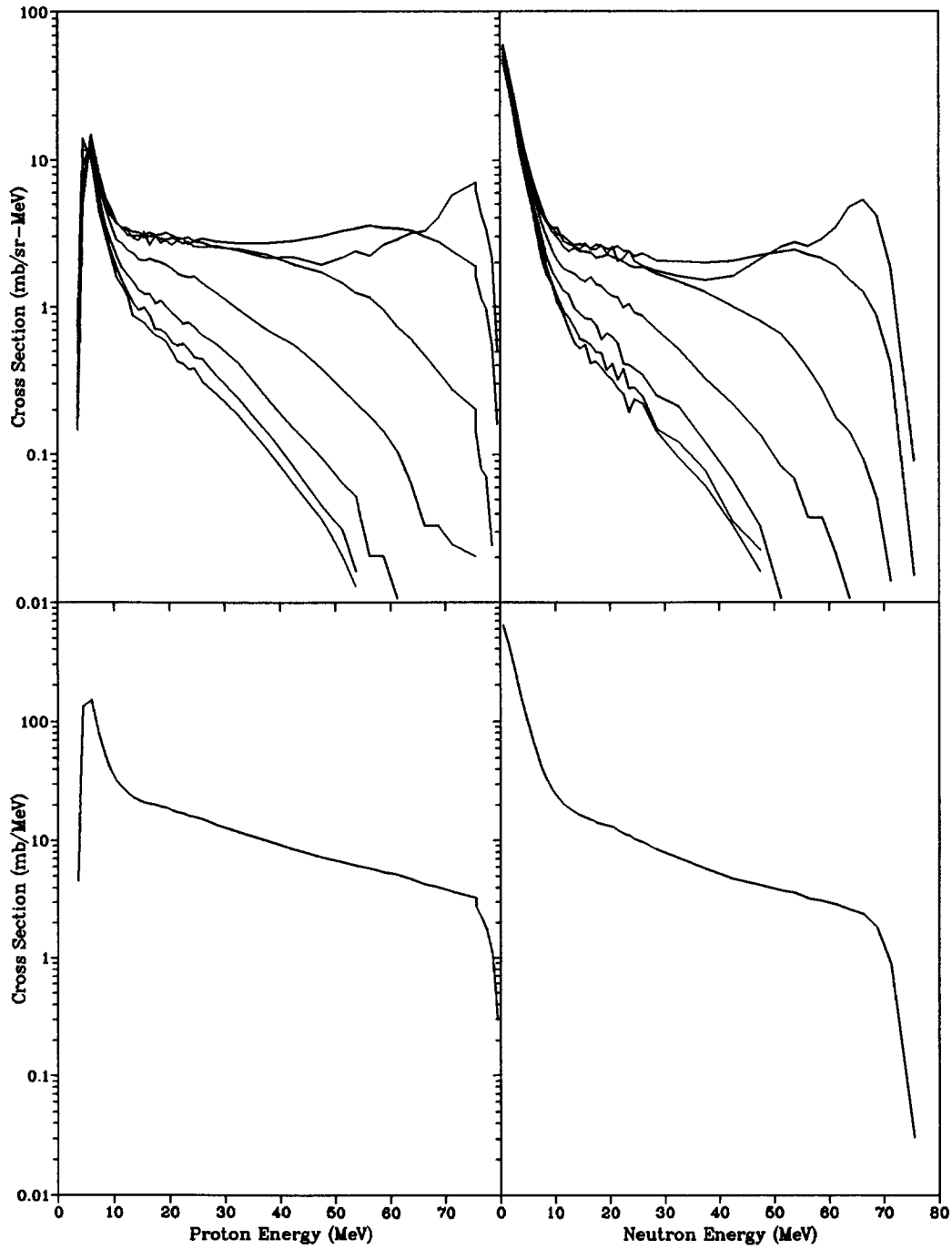

Figure 3: 80 MeV protons on ^{90}Zr. Upper left: proton emission spectrum at 11° , 25° , 45° , 69° , 95° , 120° , and 145° . Upper right: neutron emission spectrum at same angles. Lower left: angle integrated proton emission spectrum. Lower right: angle integrated neutron emission spectrum.

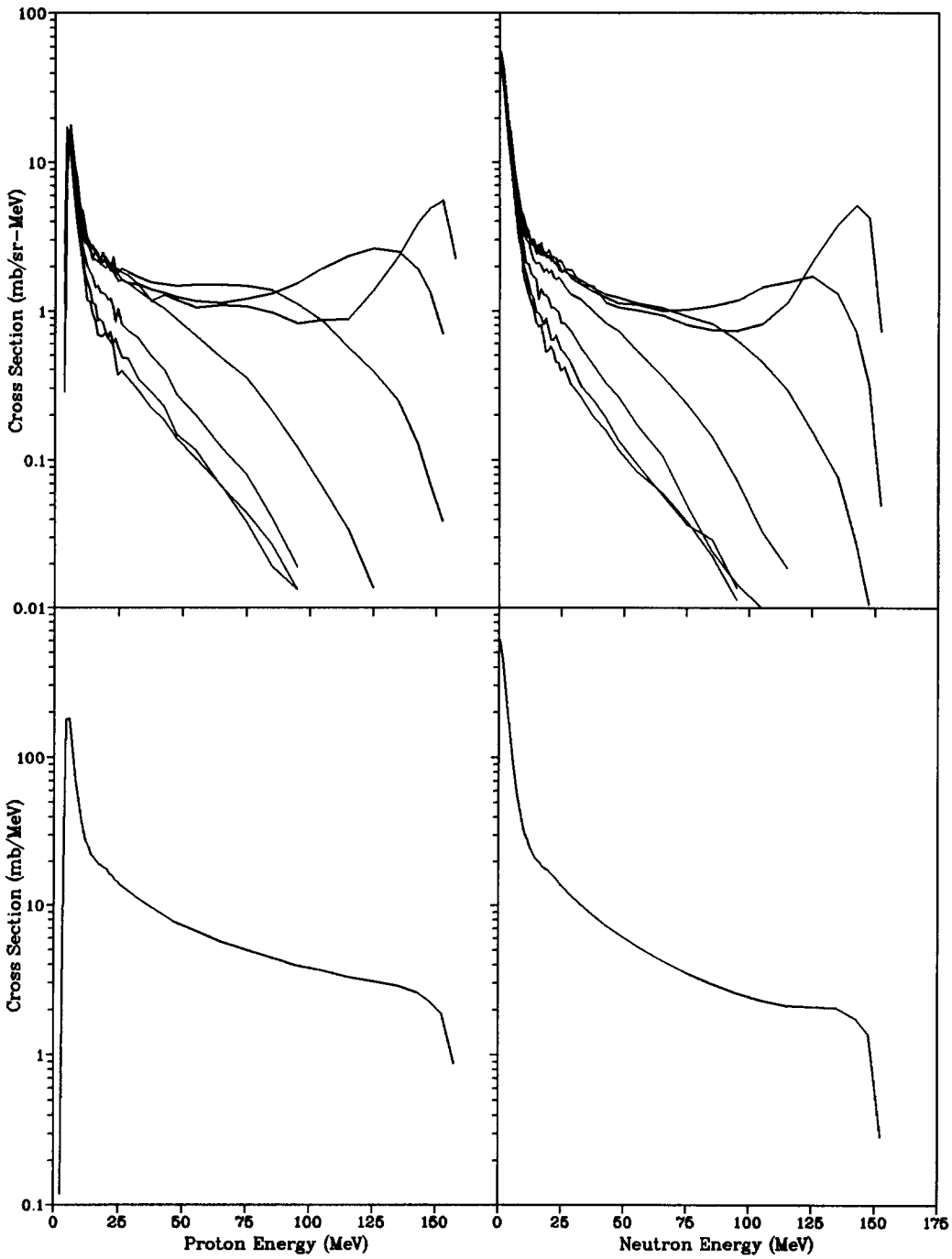

Figure 4: 160 MeV protons on ^{90}Zr. Upper left: proton emission spectrum at 11° , 25° , 45° , 69° , 95° , 120° , and 145° . Upper right: neutron emission spectrum at same angles. Lower left: angle integrated proton emission spectrum. Lower right: angle integrated neutron emission spectrum.

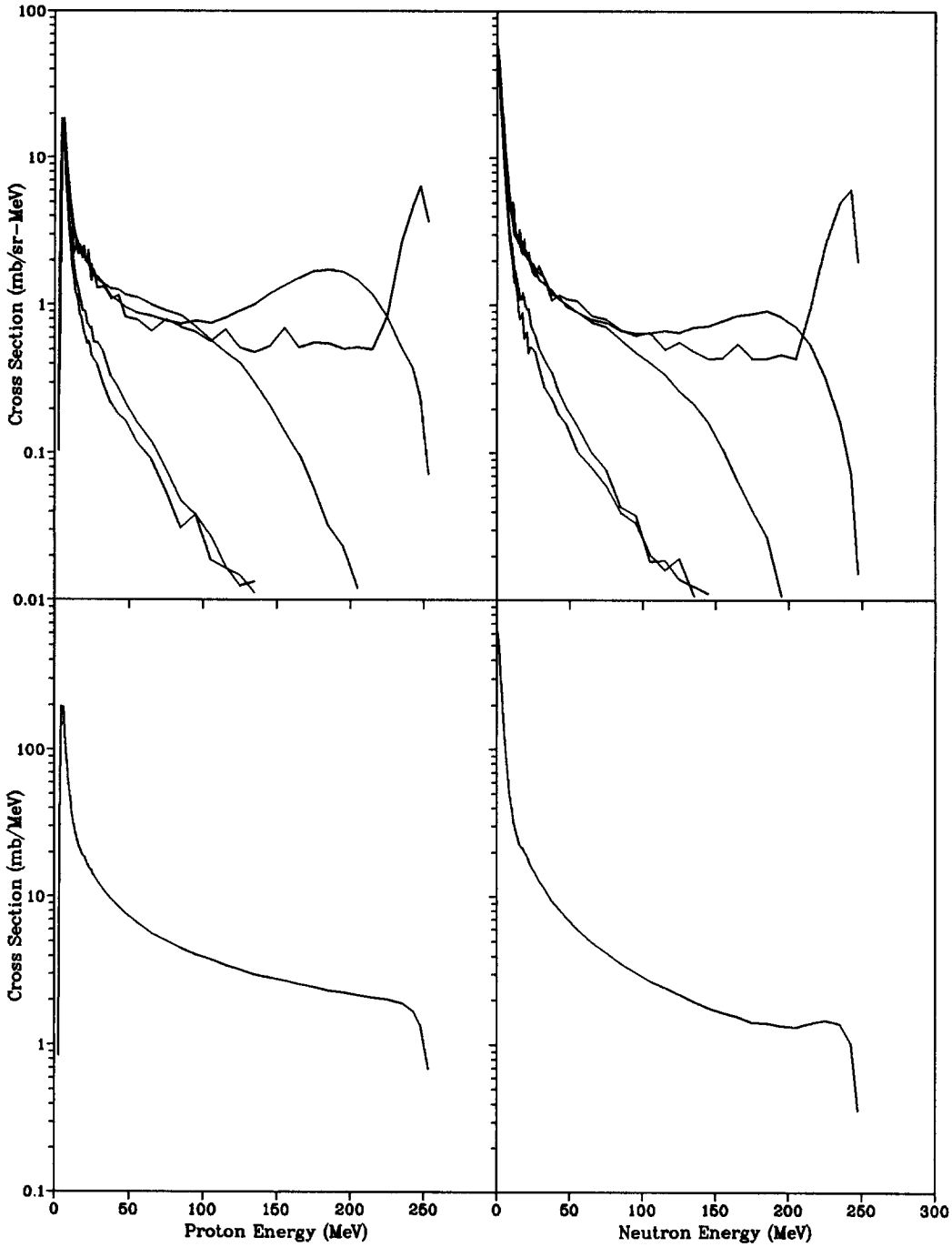

Figure 5: 256 MeV protons on ^{90}Zr. Upper left: proton emission spectrum at 7.5° , 30° , 60° , 120° , and 150° . Upper right: neutron emission spectrum at same angles. Lower left: angle integrated proton emission spectrum. Lower right: angle integrated neutron emission spectrum.

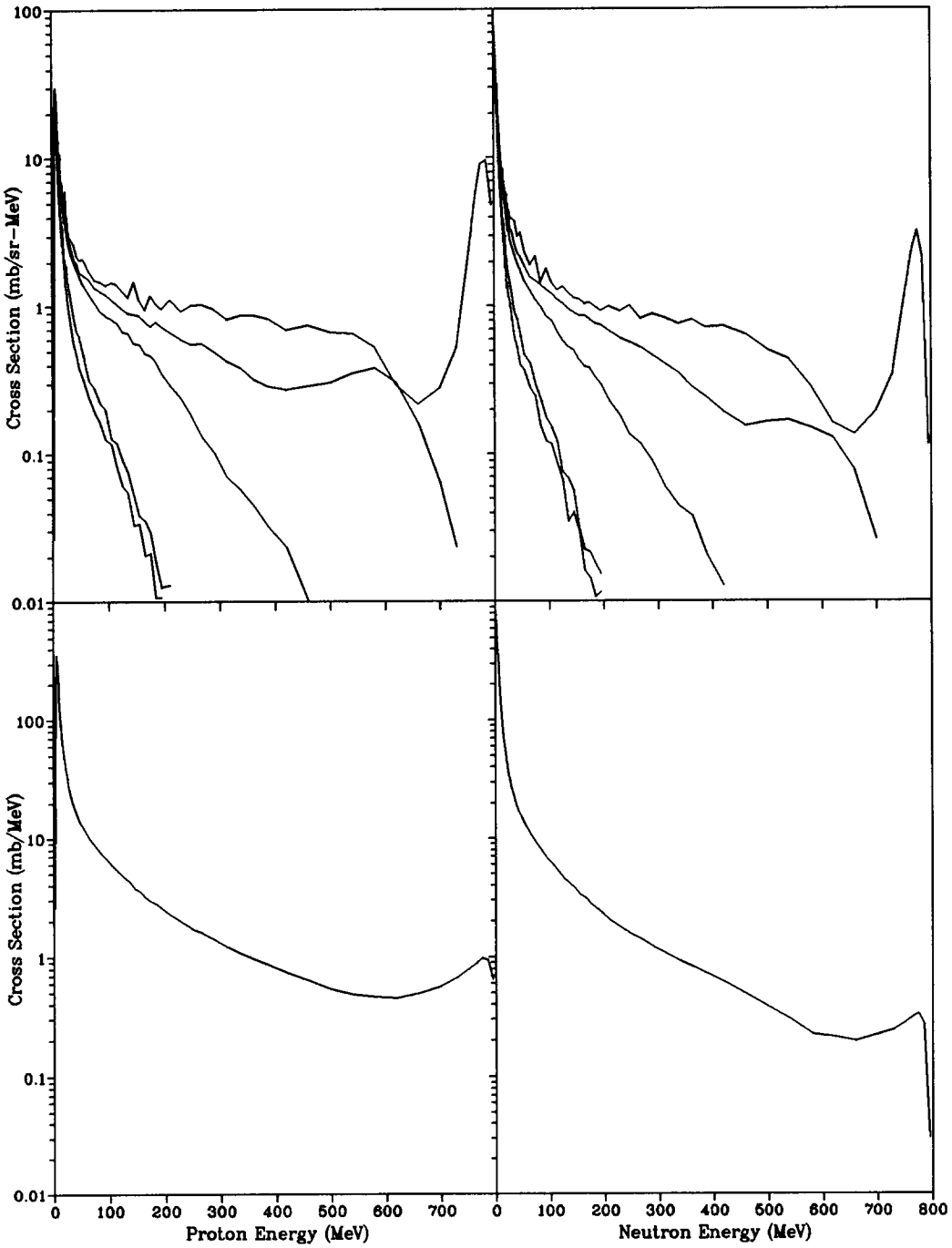

Figure 6: 800 MeV protons on ^{90}Zr. Upper left: proton emission spectrum at 7.5° , 30° , 60° , 120° , and 150° . Upper right: neutron emission spectrum at same angles. Lower left: angle integrated proton emission spectrum. Lower right: angle integrated neutron emission spectrum.

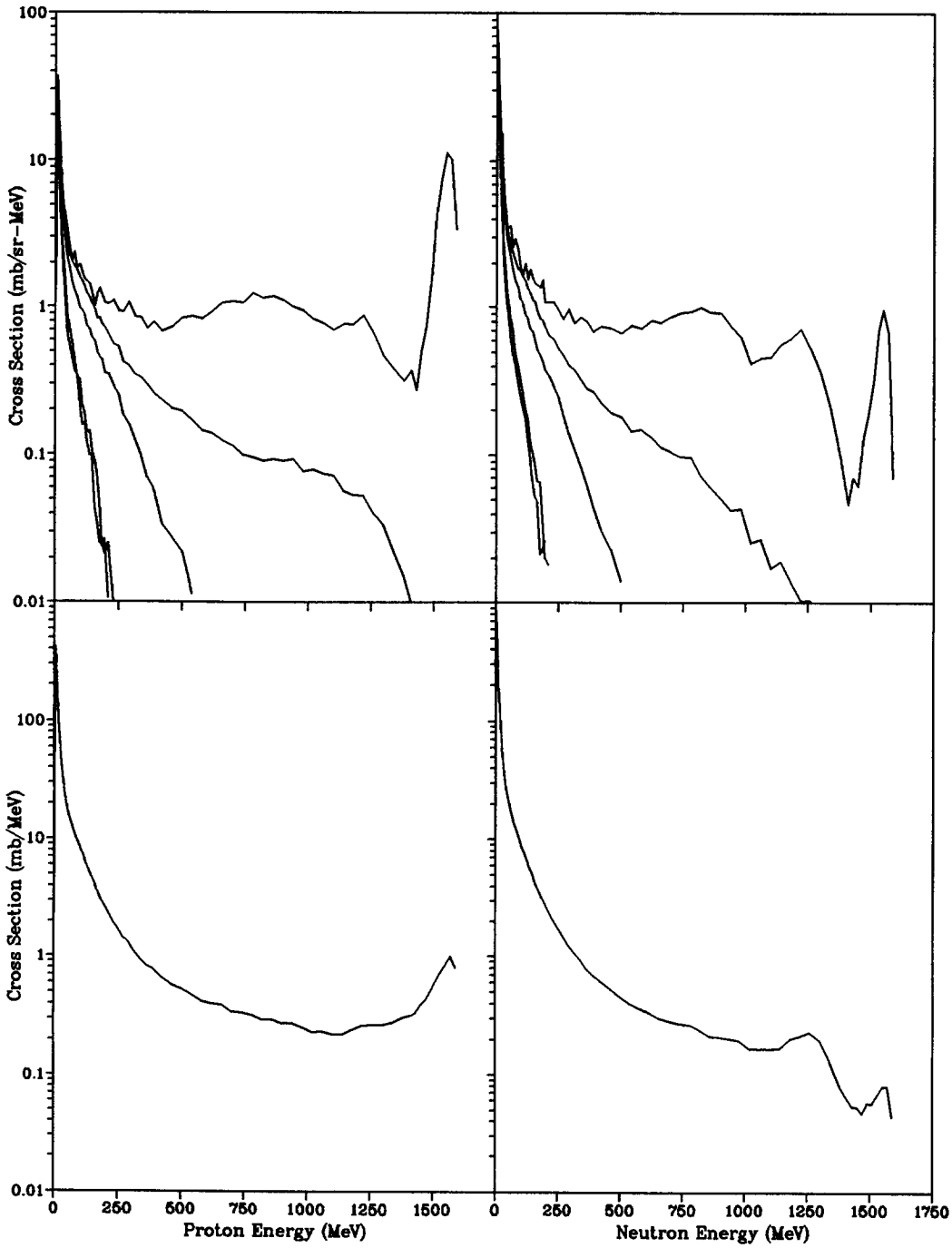

Figure 7: 1600 MeV protons on ^{90}Zr. Upper left: proton emission spectrum at 7.5° , 30° , 60° , 120° , and 150° . Upper right: neutron emission spectrum at same angles. Lower left: angle integrated proton emission spectrum. Lower right: angle integrated neutron emission spectrum.

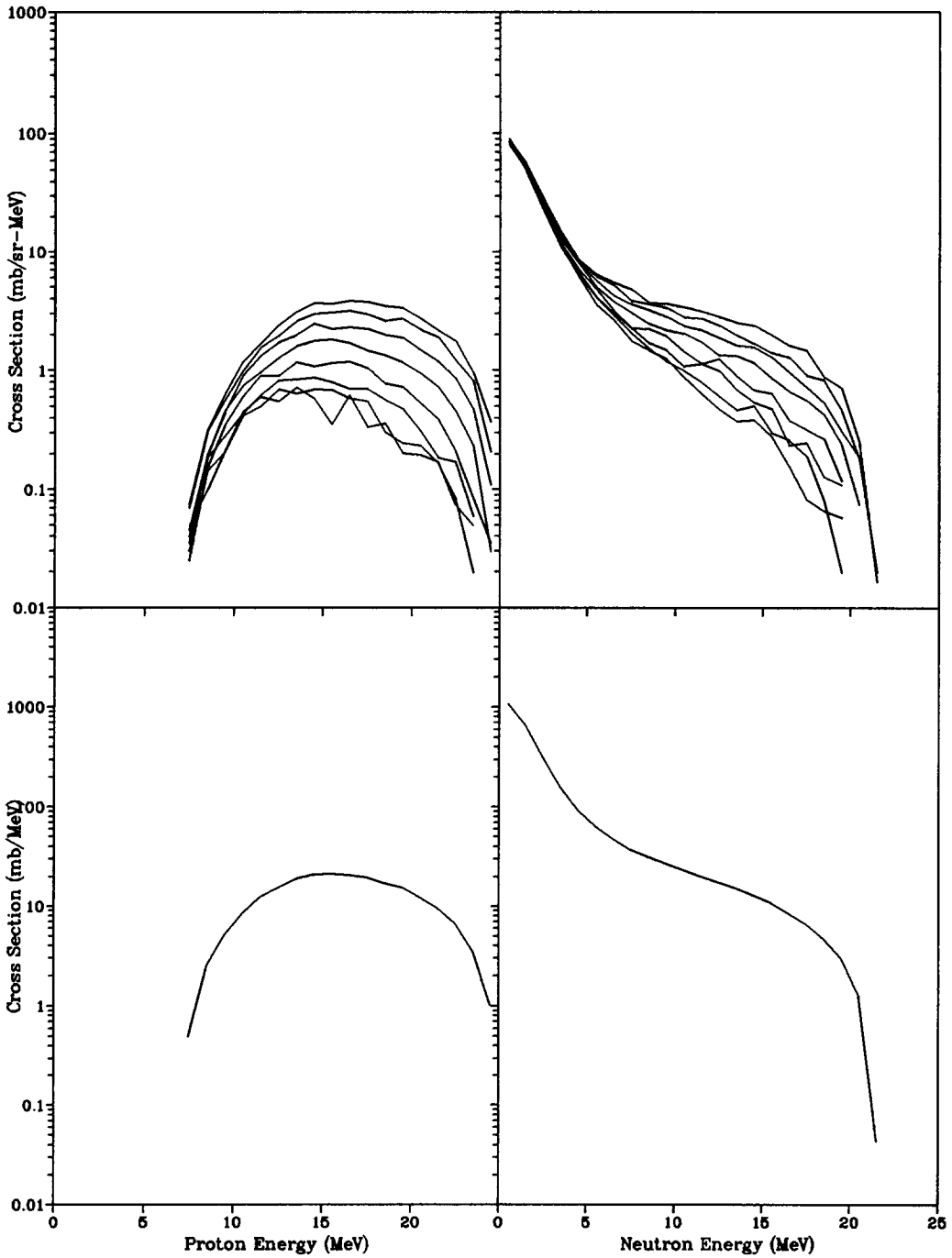

Figure 8: 25 MeV protons on ^{208}Pb. Upper left: proton emission spectrum at 20° , 40° , 60° , 80° , 100° , 120° , 140° , and 160° . Upper right: neutron emission spectrum at same angles. Lower left: angle integrated proton emission spectrum. Lower right: angle integrated neutron emission spectrum.

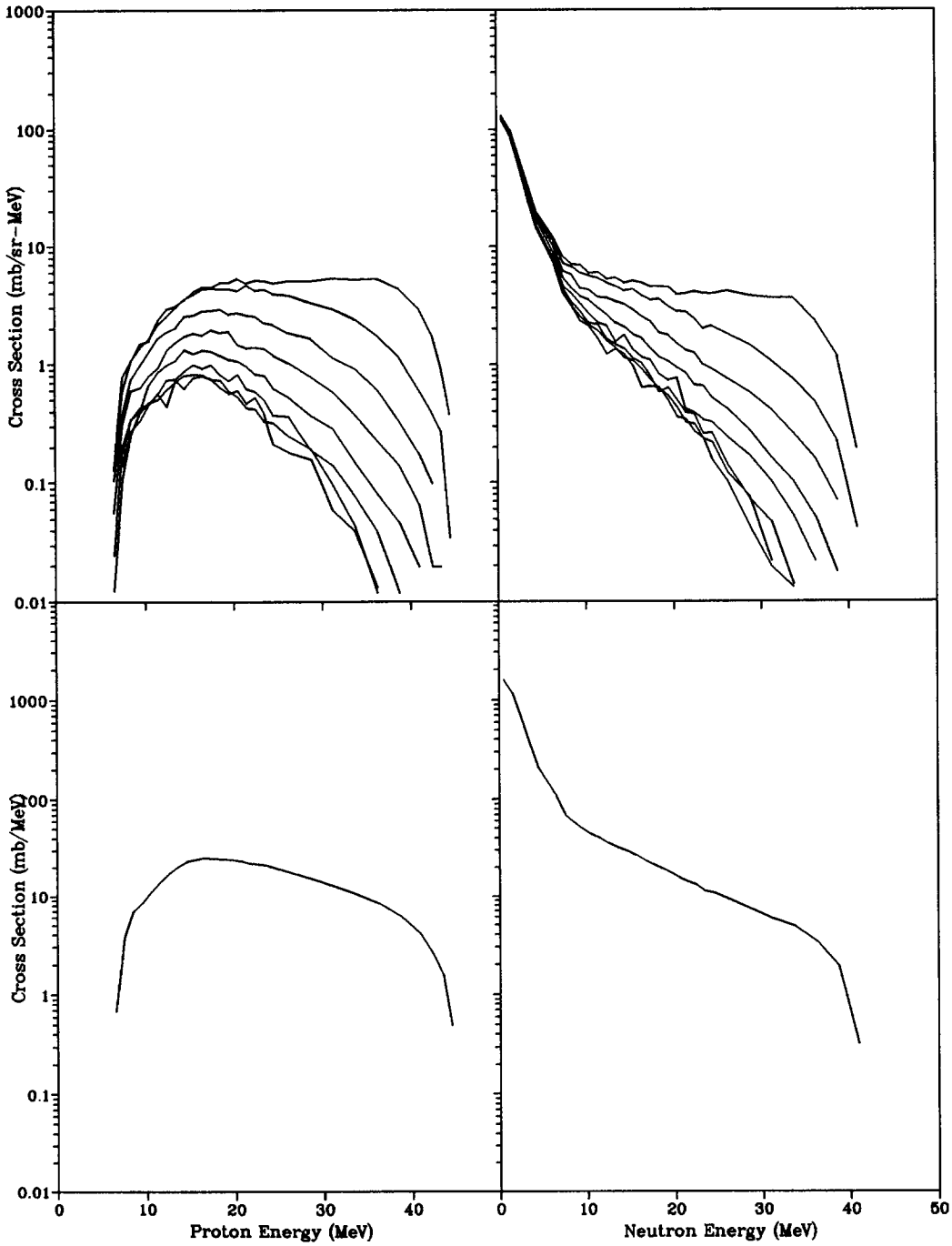

Figure 9: 45 MeV protons on ^{208}Pb. Upper left: proton emission spectrum at 20° , 40° , 60° , 80° , 100° , 120° , 140° , and 160° . Upper right: neutron emission spectrum at same angles. Lower left: angle integrated proton emission spectrum. Lower right: angle integrated neutron emission spectrum.

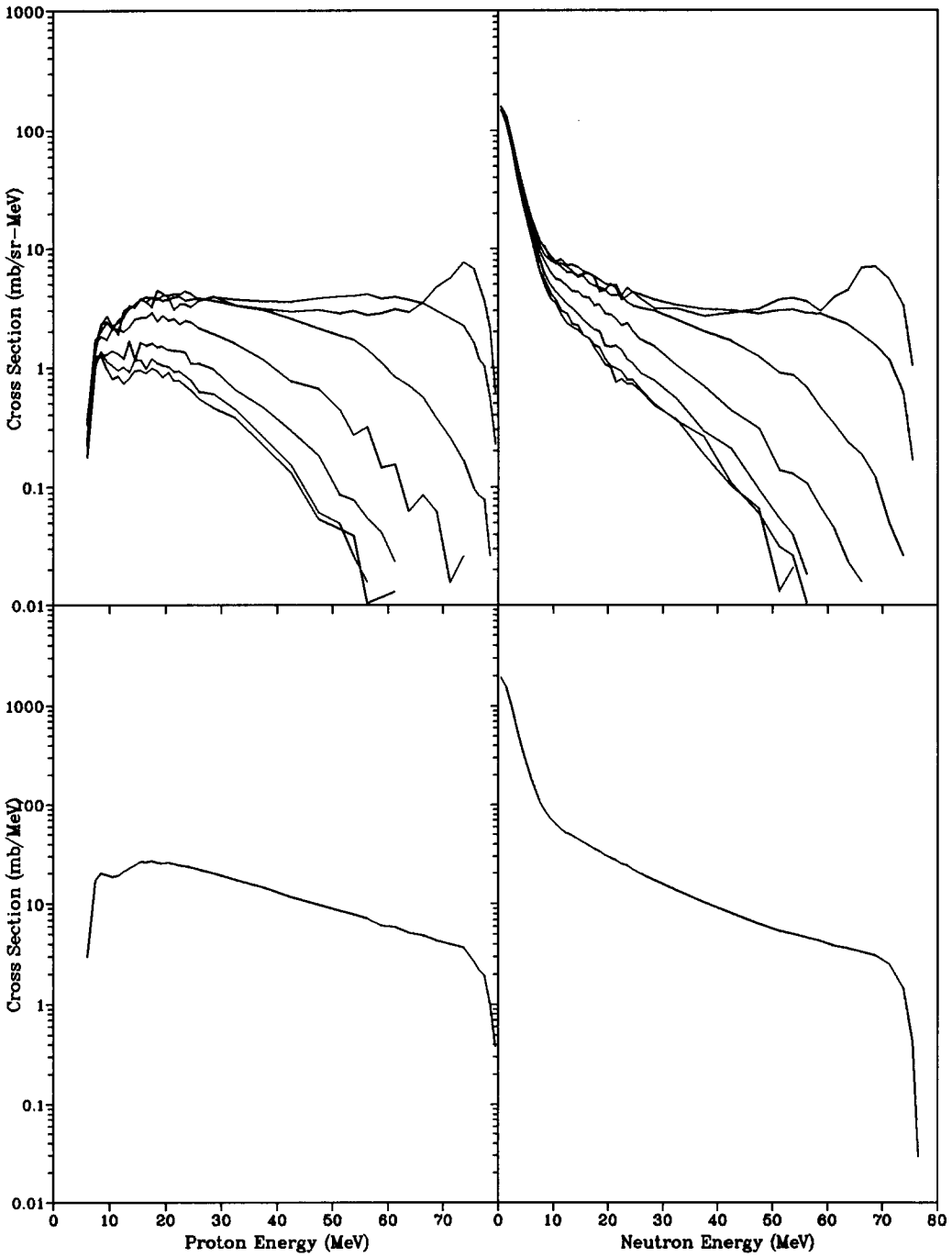

Figure 10: 80 MeV protons on ^{208}Pb. Upper left: proton emission spectrum at 11° , 25° , 45° , 69° , 95° , 120° , and 145° . Upper right: neutron emission spectrum at same angles. Lower left: angle integrated proton emission spectrum. Lower right: angle integrated neutron emission spectrum.

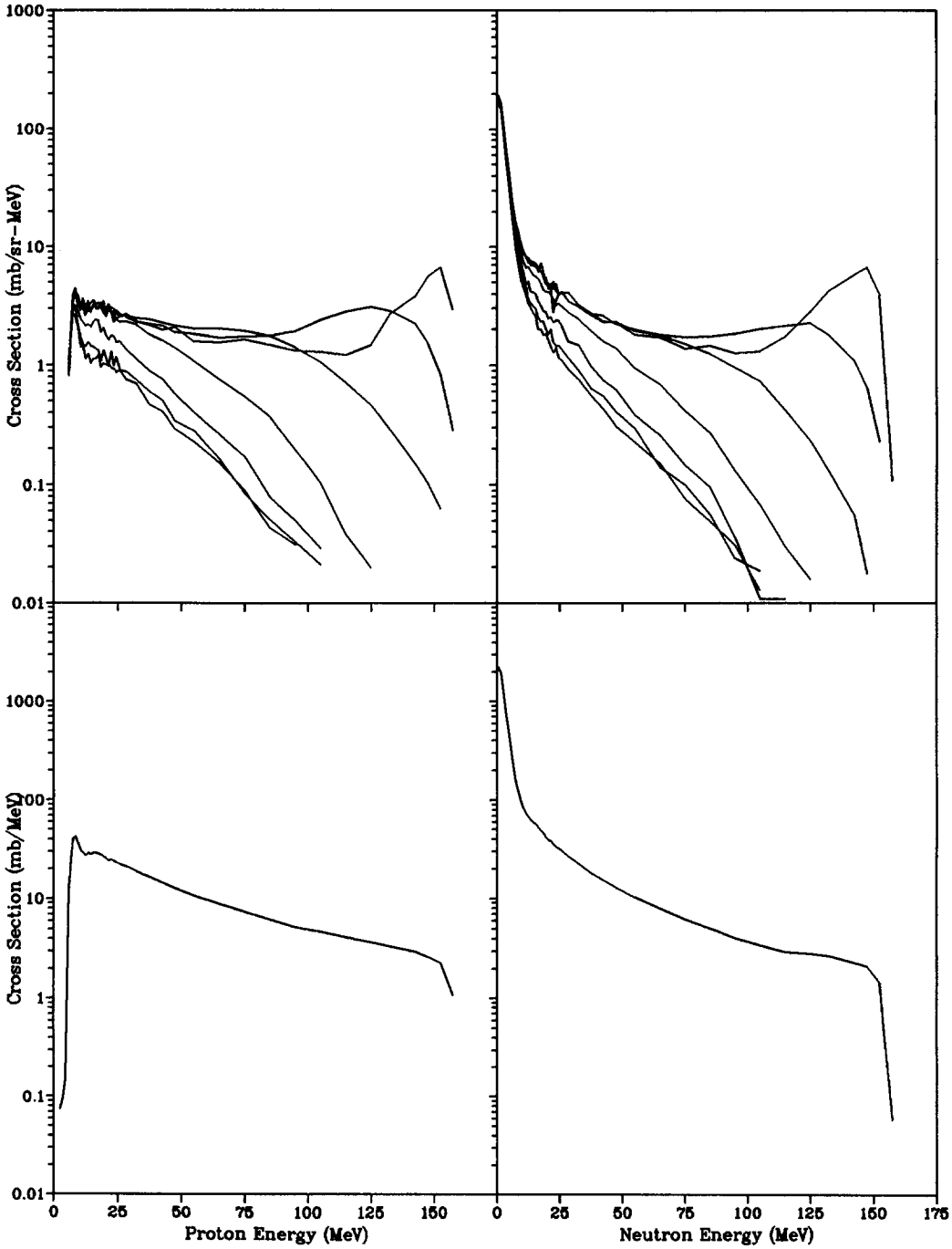

Figure 11: 160 MeV protons on ^{208}Pb. Upper left: proton emission spectrum at 11° , 25° , 45° , 69° , 95° , 120° , and 145° . Upper right: neutron emission spectrum at same angles. Lower left: angle integrated proton emission spectrum. Lower right: angle integrated neutron emission spectrum.

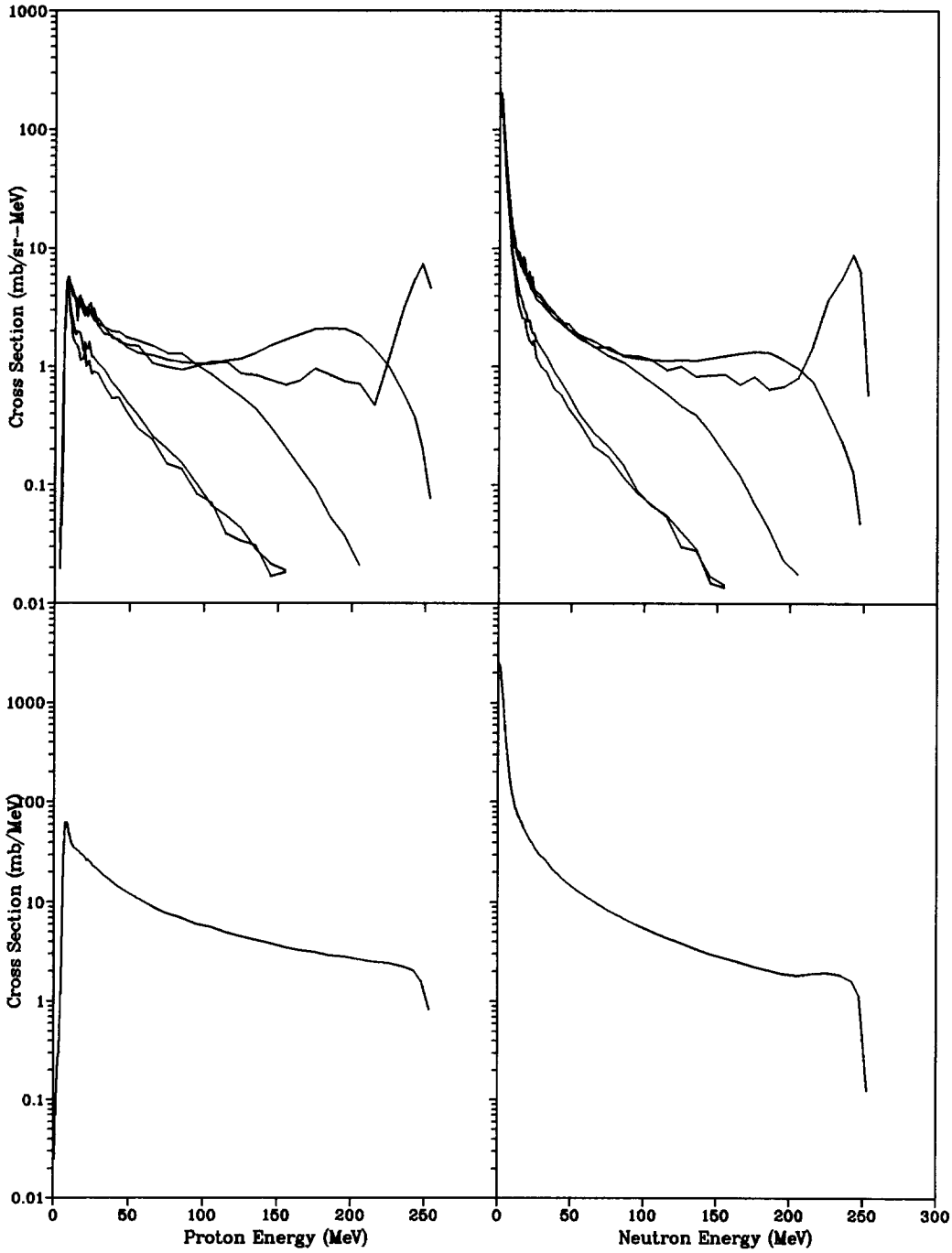

Figure 12: 256 MeV protons on ^{208}Pb. Upper left: proton emission spectrum at 7.5° , 30° , 60° , 120° , and 150° . Upper right: neutron emission spectrum at same angles. Lower left: angle integrated proton emission spectrum. Lower right: angle integrated neutron emission spectrum.

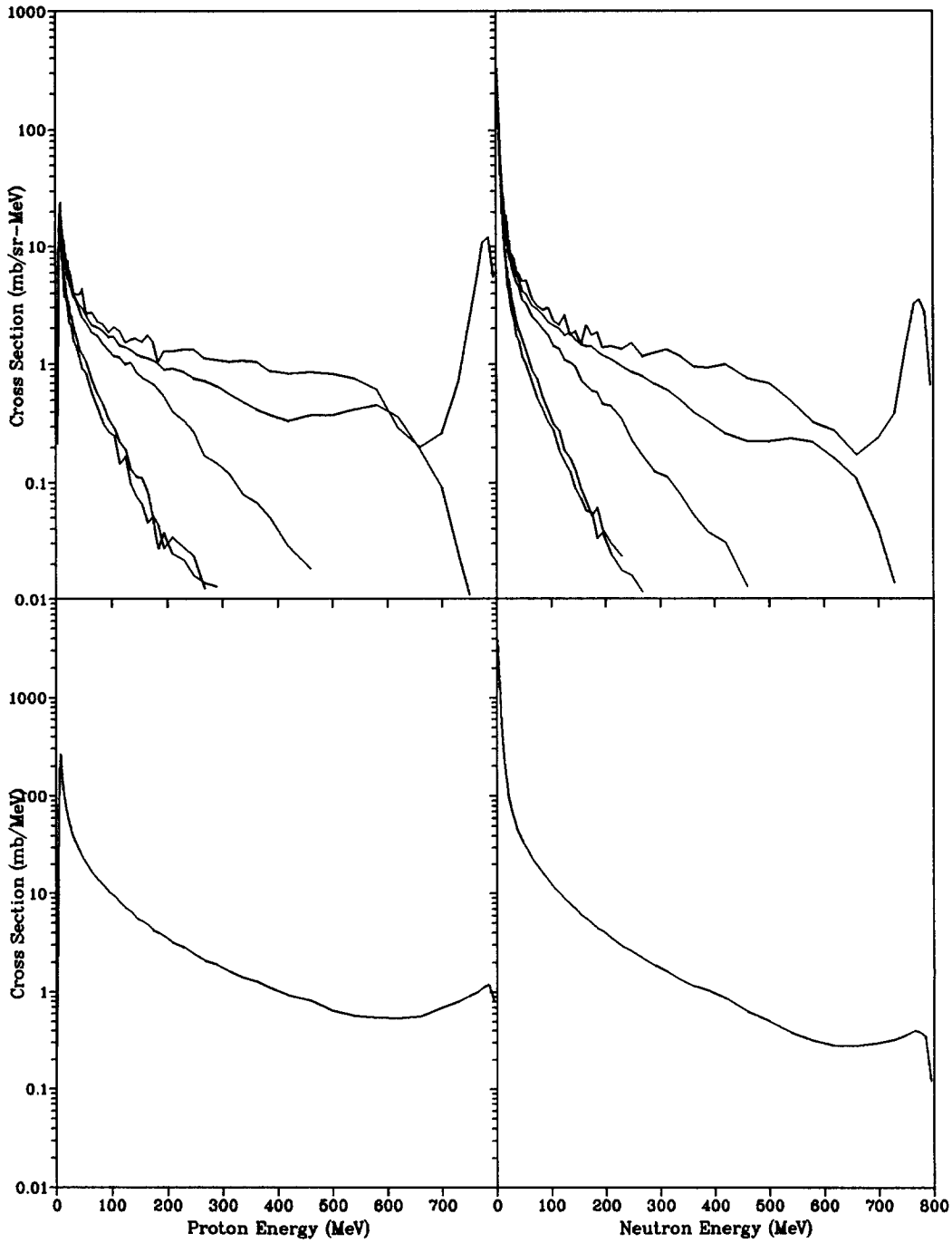

Figure 13: 800 MeV protons on ^{208}Pb. Upper left: proton emission spectrum at 7.5° , 30° , 60° , 120° , and 150° . Upper right: neutron emission spectrum at same angles. Lower left: angle integrated proton emission spectrum. Lower right: angle integrated neutron emission spectrum.

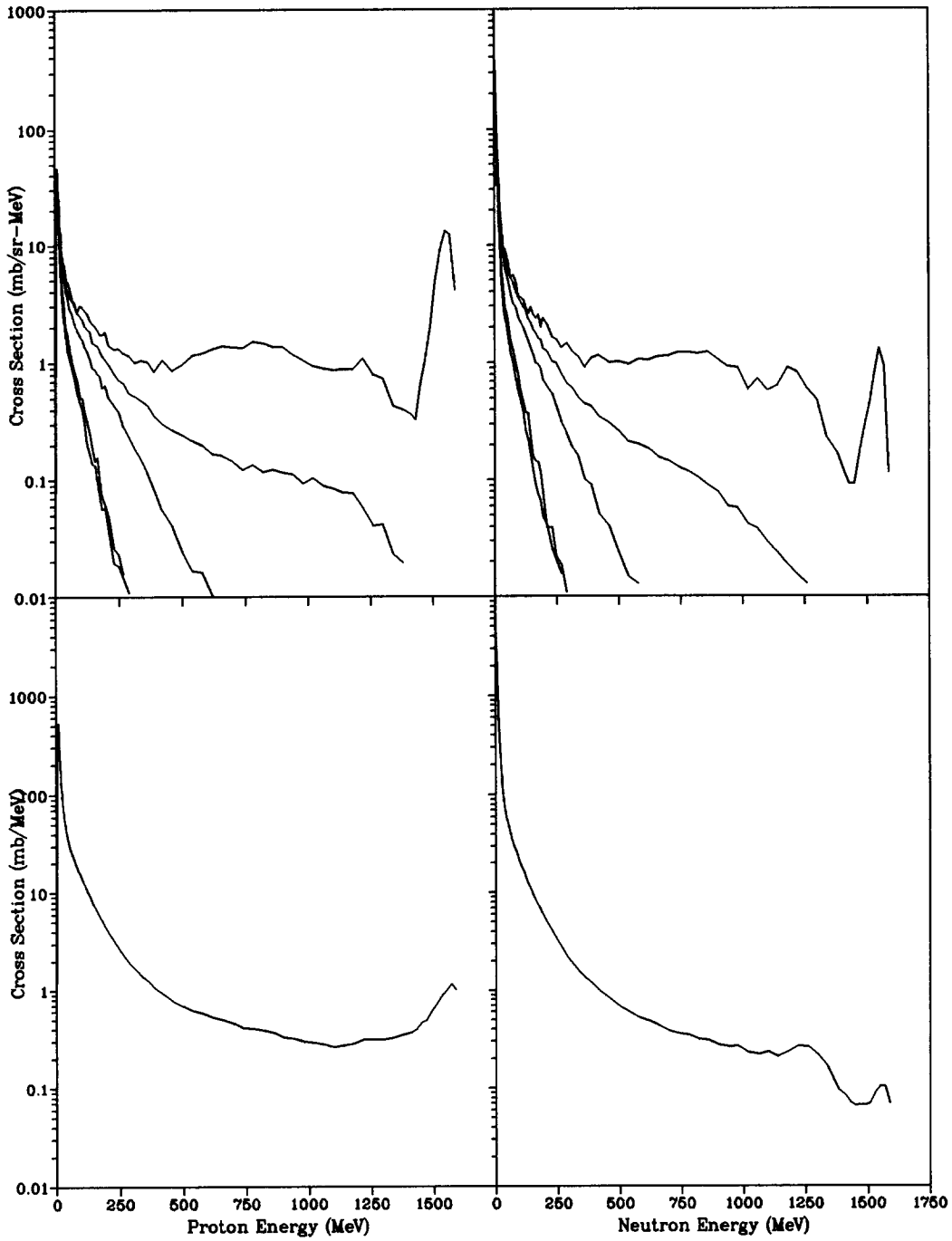

Figure 14: 1600 MeV protons on ^{208}Pb. Upper left: proton emission spectrum at 7.5° , 30° , 60° , 120° , and 150° . Upper right: neutron emission spectrum at same angles. Lower left: angle integrated proton emission spectrum. Lower right: angle integrated neutron emission spectrum.

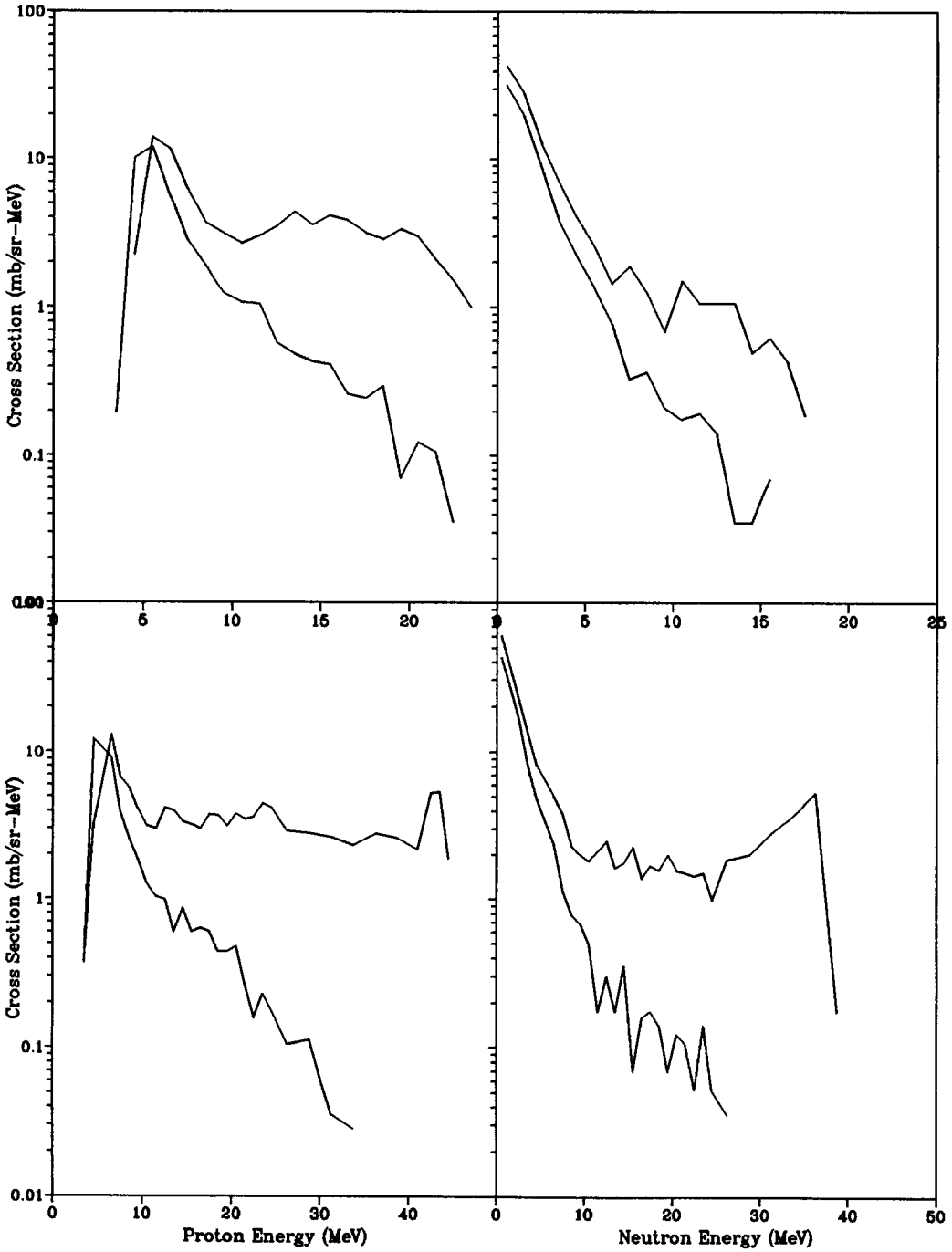

Figure 15: Upper left: 25 MeV protons on ^{90}Zr, proton emission spectrum at 0° and 180° . Upper right: neutron emission spectrum at same angles. Lower left: 45 MeV protons on ^{90}Zr, proton emission spectrum at 0° and 180° . Lower right: neutron emission spectrum at same angles.

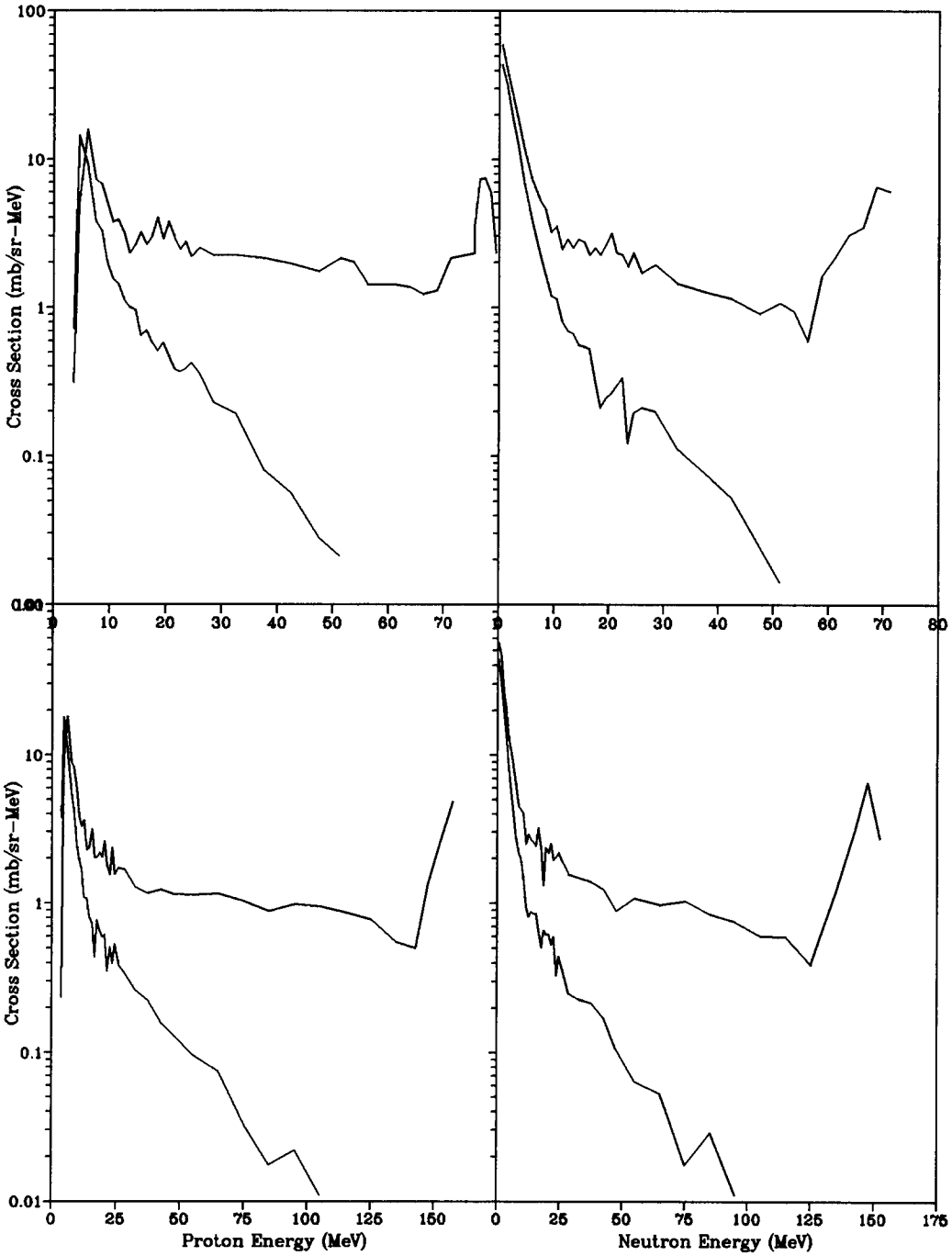

Figure 16: Upper left: 80 MeV protons on ^{90}Zr, proton emission spectrum at 0° and 180° . Upper right: neutron emission spectrum at same angles. Lower left: 160 MeV protons on ^{90}Zr, proton emission spectrum at 0° and 180° . Lower right: neutron emission spectrum at same angles.

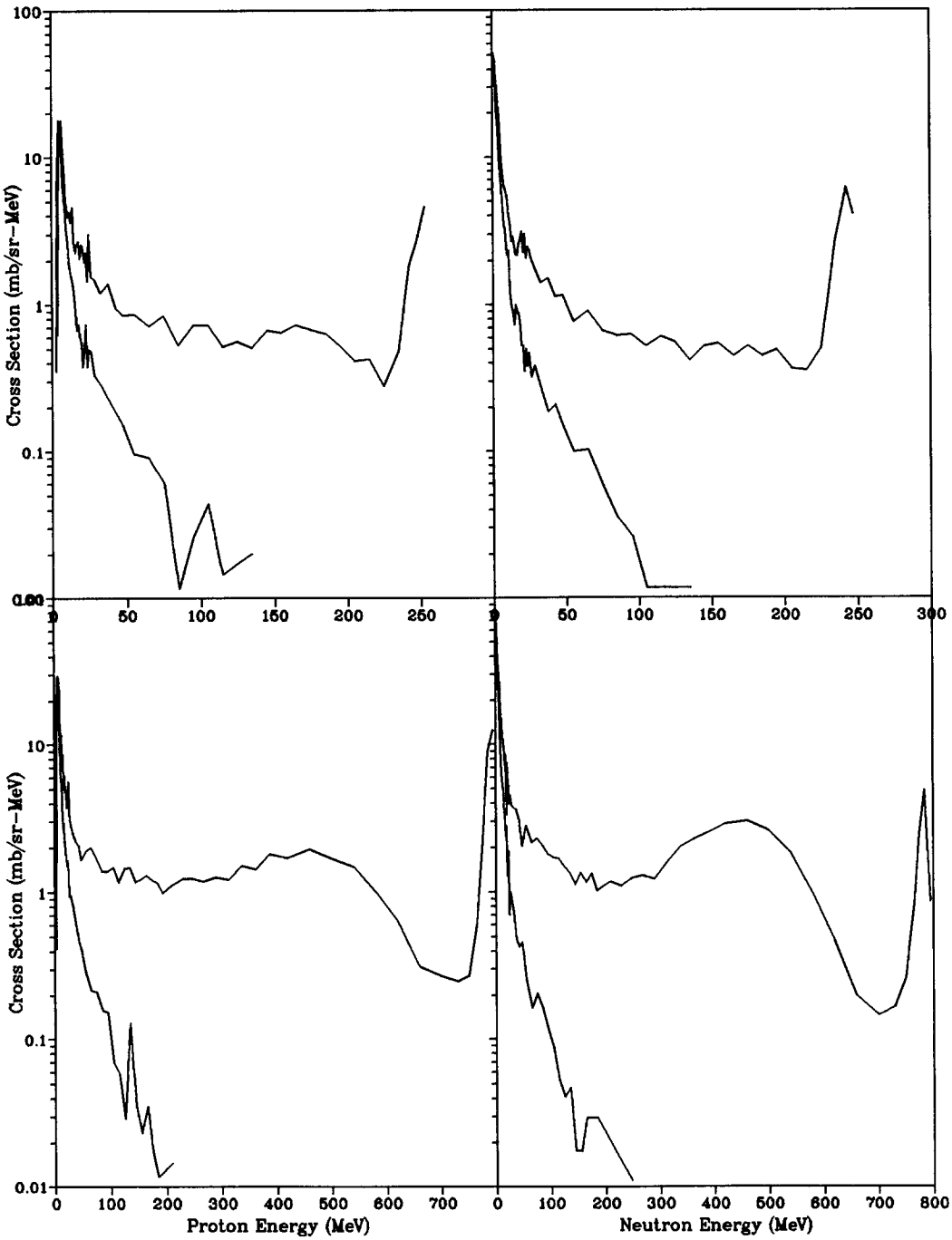

Figure 17: Upper left: 256 MeV protons on ^{90}Zr, proton emission spectrum at 0° and 180° . Upper right: neutron emission spectrum at same angles. Lower left: 800 MeV protons on ^{90}Zr, proton emission spectrum at 0° and 180° . Lower right: neutron emission spectrum at same angles.

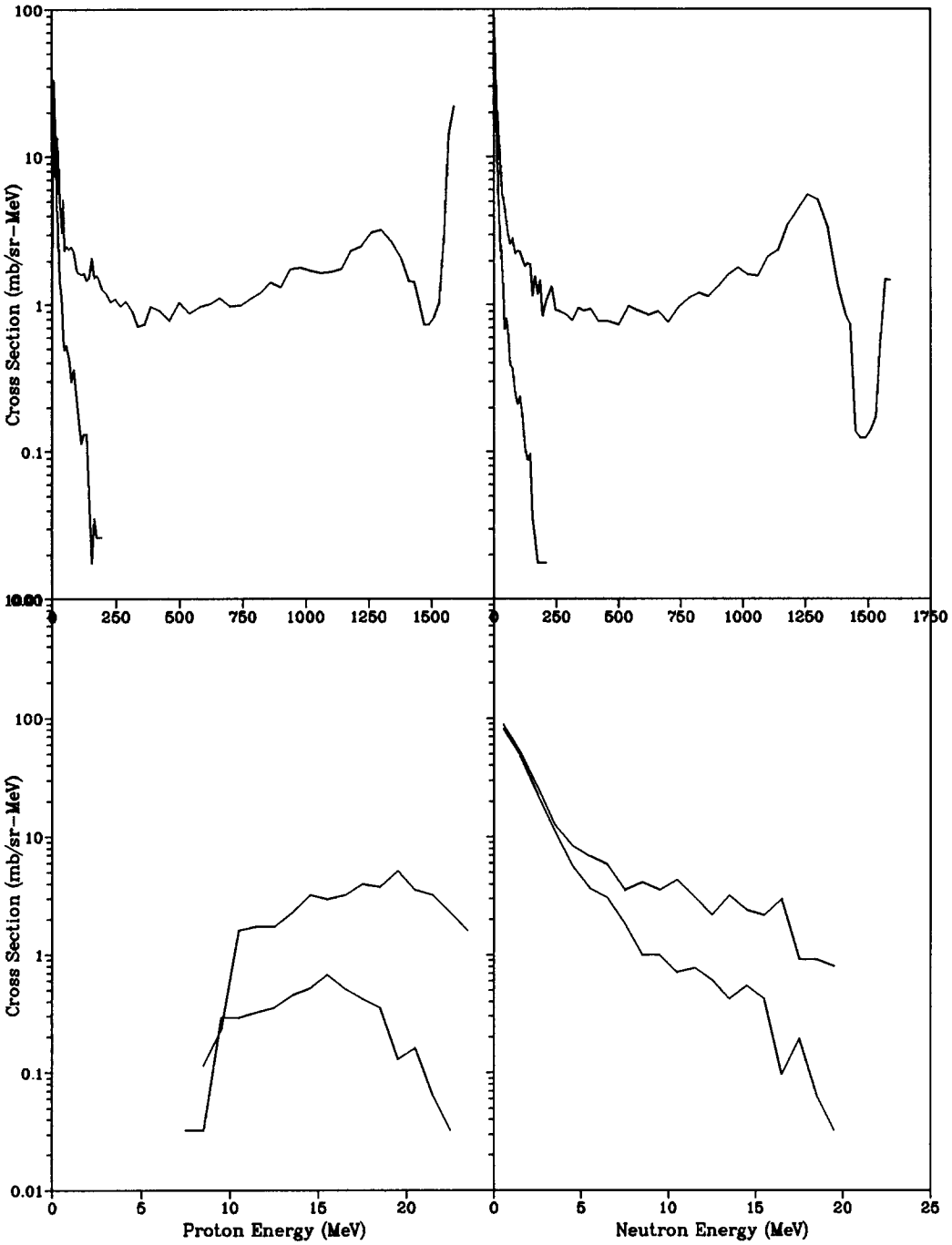

Figure 18: Upper left: 1600 MeV protons on ^{90}Zr, proton emission spectrum at 0° and 180° . Upper right: neutron emission spectrum at same angles. Lower left: 25 MeV protons on ^{208}Pb, proton emission spectrum at 0° and 180° . Lower right: neutron emission spectrum at same angles.

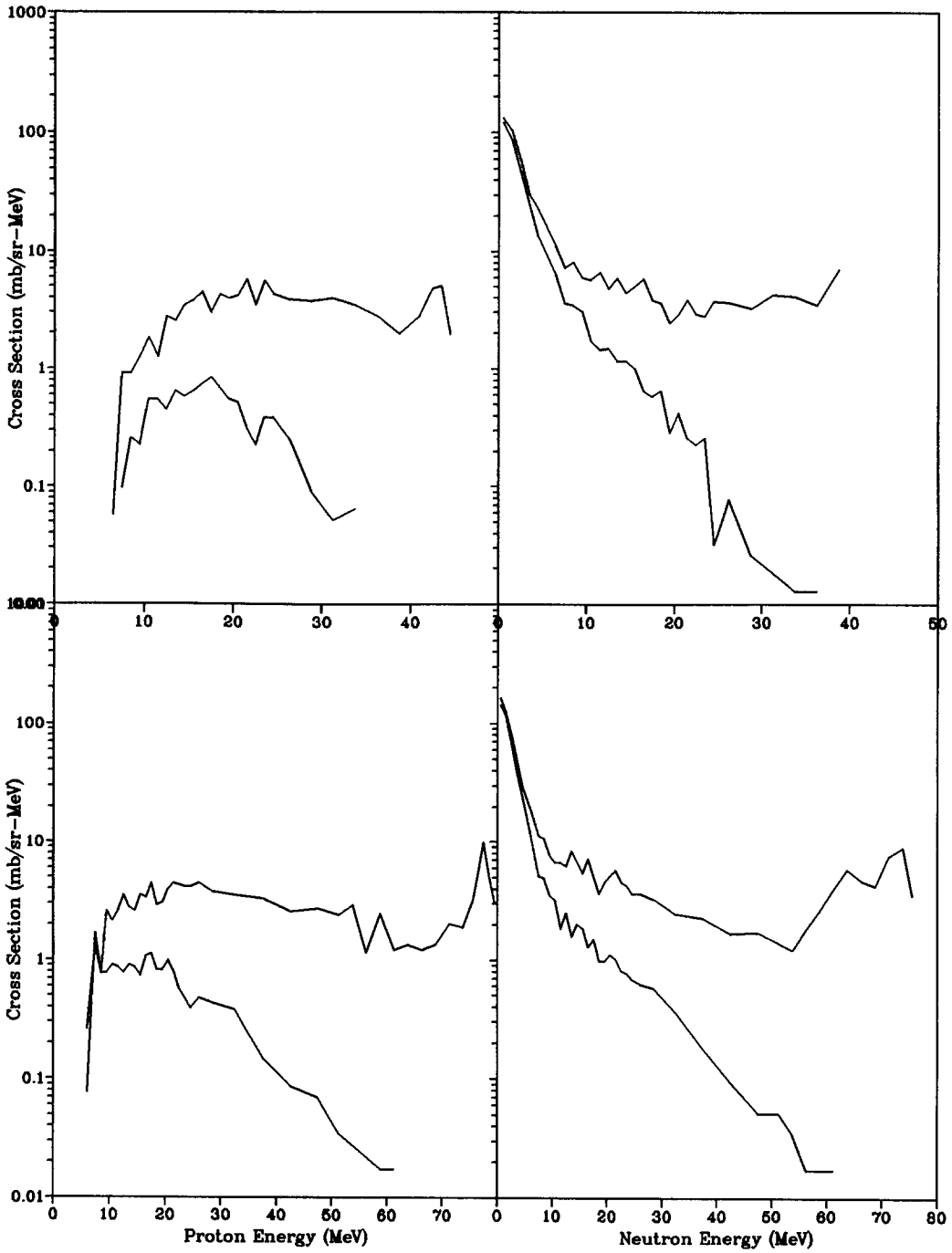

Figure 19: Upper left: 45 MeV protons on ^{208}Pb, proton emission spectrum at 0° and 180° . Upper right: neutron emission spectrum at same angles. Lower left: 80 MeV protons on ^{208}Pb, proton emission spectrum at 0° and 180° . Lower right: neutron emission spectrum at same angles.

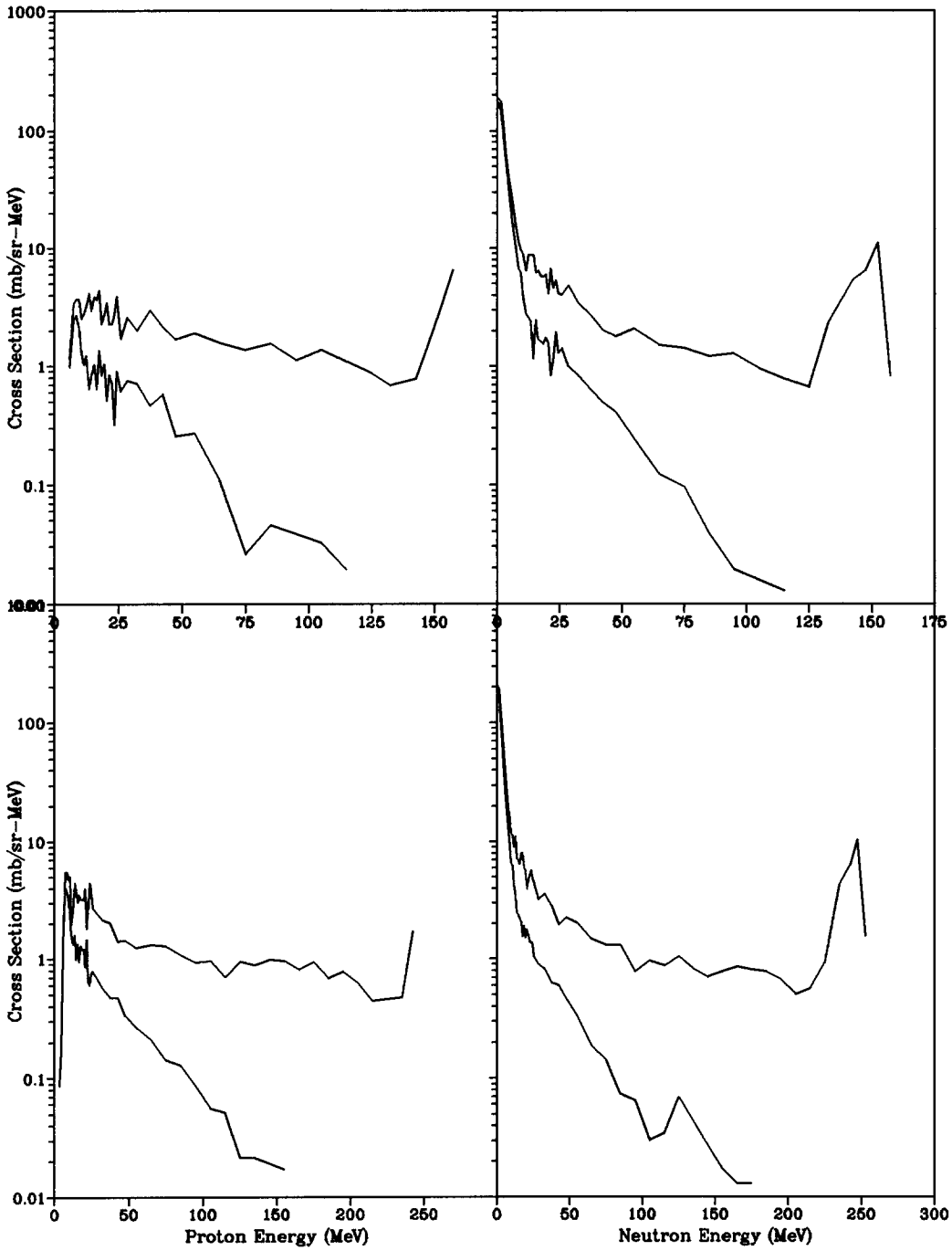

Figure 20: Upper left: 160 MeV protons on ^{208}Pb, proton emission spectrum at 0° and 180° . Upper right: neutron emission spectrum at same angles. Lower left: 256 MeV protons on ^{208}Pb, proton emission spectrum at 0° and 180° . Lower right: neutron emission spectrum at same angles.

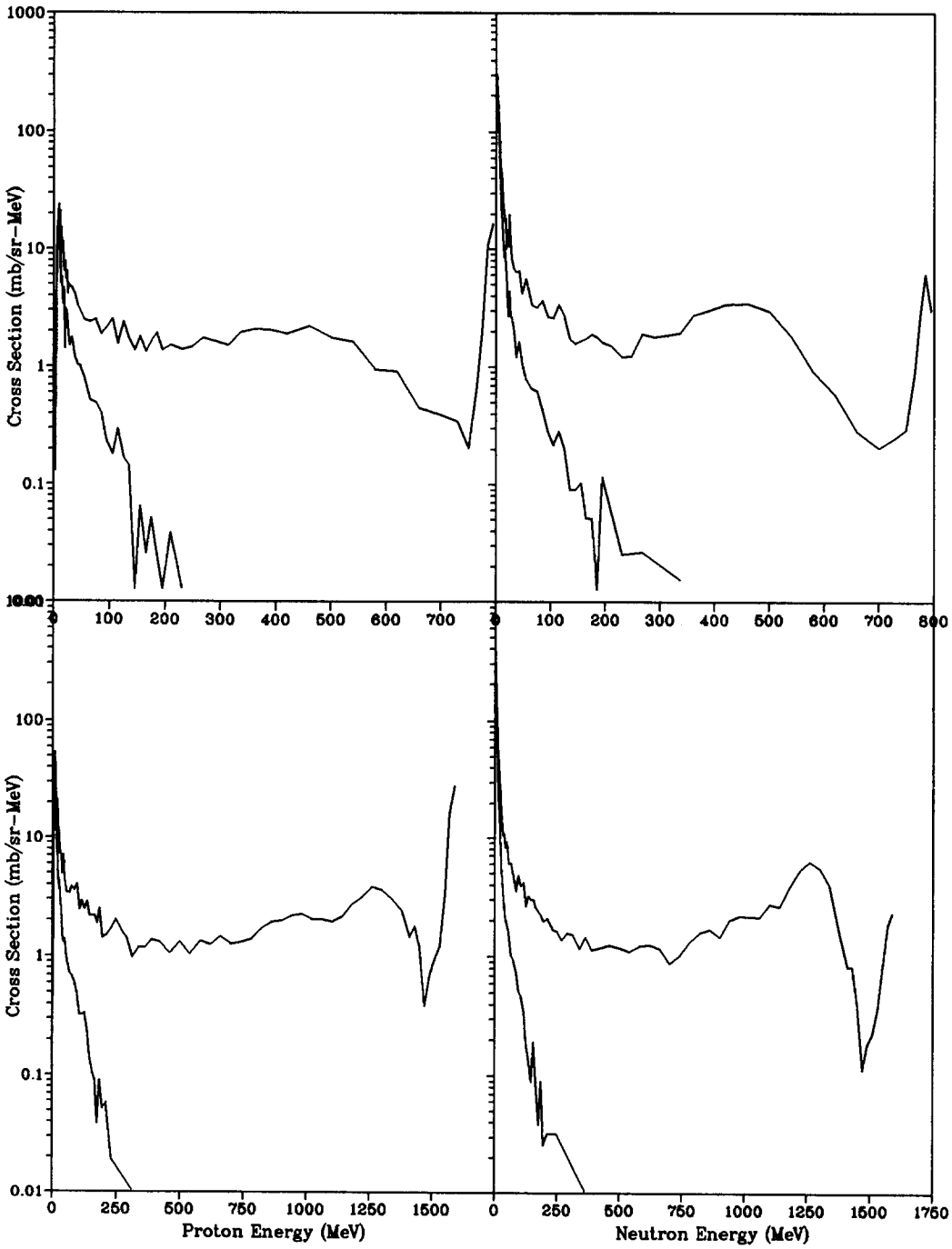

Figure 21: Upper left: 800 MeV protons on ^{208}Pb, proton emission spectrum at 0° and 180° . Upper right: neutron emission spectrum at same angles. Lower left: 1600 MeV protons on ^{208}Pb, proton emission spectrum at 0° and 180° . Lower right: neutron emission spectrum at same angles.